JPE 19-4-9

https://doi.org/10.6113/JPE.2019.19.4.934
ISSN(Print): 1598-2092 / ISSN(Online): 2093-4718

Current Sharing Method Based on Optimal Phase Shift Control for Interleaved Three-Phase Half Bridge LLC Converter with Floating Y-Connection

Lin Shi*, Bangyin Liu†, and Shanxu Duan*

†,*State Key Laboratory of Advanced Electromagnetic Engineering and Technology,
School of Electrical and Electronic Engineering, Huazhong University of Science and Technology, Wuhan, China

Abstract

A current balance problem exists in multi-phase LLC converters due to the resonant parameter tolerance. This paper presents a current balancing method for interleaved three-phase half bridge LLC converters. This method regulates the phase shift angle of the driving signals between the three phases based on a converter with a floating Y-connection. The floating midpoint voltage has different influences on each phase current and makes the three-phase current balance performance better than midpoint non-floating systems. Phase shift control between modules can further regulate the midpoint voltage. Then three phase current sharing is realized without adding extra components. The current distributions in a midpoint non-floating system and a midpoint floating system are compared. Then the principle and implementation of the proposed control strategy are analyzed in detail. A 3kW prototype is built to verify the validity and feasibility of the proposed method.

Key words: Current sharing, Interleaved LLC converter, Phase shift control, Three-phase LLC converter, Y-connection

I. INTRODUCTION

LLC resonant converters have been widely used for isolated DC/DC applications such as servers, electric vehicles, renewable power systems, etc., due to its attractive features: high efficiency, high power density and soft switching characteristic. Nowadays, LLC converters need to deliver more and more power. Under this condition, the conduction loss is greatly increased in low voltage and high current applications. As a result, the system becomes prone to overheating and its efficiency is affected. In addition, a bulk capacitor is necessary at the output side due to the injection of rectified sinusoidal current. Thus, the interleaved multi-phase LLC topology is a good choice for reducing both the conduction loss and the volume of the output capacitor [1]-[9].

Manuscript received Jul. 13, 2018; accepted Mar. 17, 2019
Recommended for publication by Associate Editor Yijie Wang.
†Corresponding Author: lby@hust.edu.cn
Tel: +86-27-87558427, Fax:+86-27-87559303, Huazhong Univ. of Sci. and Tech.
*State Key Lab. of Adv. Electromagn. Eng. and Tech., Sch. of Electr. and Electron. Eng., Huazhong Univ. of Sci. and Tech., China

In a multi-phase LLC converter, all of the sub-modules are required to work at the same switching frequency in case of a beat frequency on the output capacitor. However, due to parameter tolerance among the different phases, the currents of each phase differ. The authors of [10] presented the current distribution for a two-phase interleaved LLC system with a different resonant parameter tolerance. It demonstrated that with a mere 2.5% resonant inductance and capacitance mismatch, two modules transmit extremely high unbalanced currents around the resonant frequency.

Previous studies on the current sharing of interleaved LLC converters can be classified into hardware structure optimizations and control method optimizations [11]-[24]. In [11], the voltage sources of each module are independent and controlled separately. Thus, the current sharing is realized by changing the respective bus voltage. In [12], the input series output parallel (ISOP) structure is used. This structure can naturally realize current sharing. However, the currents for each of the modules are higher than currents in the input parallel system when the same output power is required. The authors of [13] proposed a new two-phase LLC converter topology with natural current sharing by adding an extra

flying capacitor. The equivalent input voltages of the two phases are different because of this extra component. On the other hand, a method which can change the resonant parameters in real-time is utilized to compensate for their natural mismatch. In [14], a variable resonant inductor is designed. In addtion, a series switch and capacitor branch are added in parallel with the resonant capacitor in [15]. Hence, the equivalent capacitance of the resonant tank varies with the different duty ratios of the additional switch. In [16] and [17], coupled inductors are added between phases to change the equivalent resonant inductance.

In addition to methods of modifying the system structure, some researchers are focus on the methods of control or simply changing the connection. In [18] and [19], a frequency controlled current balancing method was proposed. Since the operating point is determined by fixed parameters, the system cannot be adapted to the change of the input and output voltage. In [20] and [21], the inductors and capacitors of each phase are simply paralleled to balance the current. However, the interleaving effect cannot be achieved. The method of a phase shift inside one phase is used in [22]-[24]. This method is used with systems that have at least four switches in each phase. The main disadvantage is that soft-switching of the lagging bridge switches is difficult to achieve, especially with a large shift angle or a high operating frequency. In such cases, the switching loss and EMI performance are influenced. The authors of [25] proposed a method that involved floating the midpoint of three-phase half-bridge LLC converters in a Y-connection and regulating the phase angle of the driving signals among three modules. However, the reason why LLC converters in a Y-connection have the current sharing capacity and the concrete control strategy of the phase shift control are not investigated.

A three-phase LLC converter in a Y-connection has the advantage that no additional components are required when realizing current sharing. Meanwhile, the benefits of the interleaved control strategy are retained. In this paper, the reason why this structure has inherent current balance capacity with resonant parameter tolerance is analyzed under general cases. A control strategy for realizing current sharing based on the phase shift control between modules is proposed. In addition, its principle and controlling rules are elaborated.

The remainder of this paper is organized as followed. In Section II, the steady-state current distribution characteristics of a midpoint non-floating system (MPNFS) with resonant parameter tolerance are analyzed based on FHA (Fundamental Harmonic Approximation). Then the current distribution in a midpoint floating system (MPFS) is compared with that in the MPNFS. In Section III, the influence of the additional phase shift angle of the driving signals is analyzed. Then a practical control strategy is proposed to realize three phase current sharing. Experimental results obtained with a 3kW LLC prototype are shown in Section IV. Finally, some conclusions are presented in Section V.

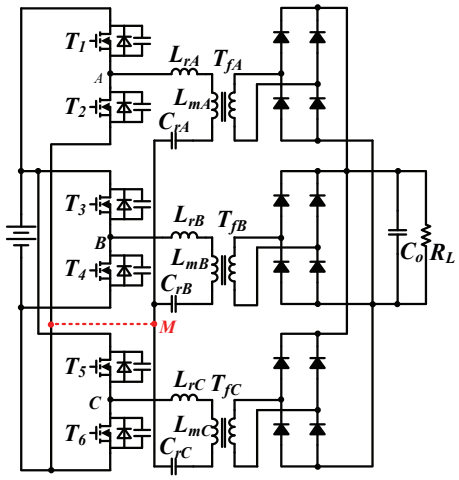

Fig. 1. Three-phase interleaving LLC Converter.

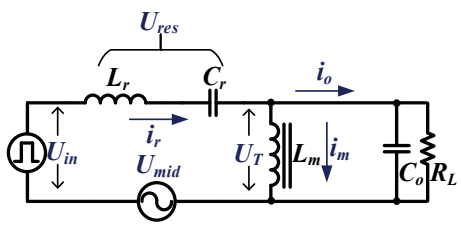

Fig. 2. Single phase equivalent circuit.

II. Calculation of Midpoint Voltage With Y-Connection Transformers

Fig. 1 shows the circuit configuration of a three-phase half bridge LLC resonant converter. T_1~T_6 are the primary Half Bridge (HB) switches of the three phases. L_{rk}, C_{rk}, and L_{mk} (k=A,B,C) are the resonant inductors, resonant capacitors and magnetizing inductors of the three phases. The three identical LLC converters are in parallel connection the switch at the same frequency but with a 120° phase-shift of their driving signals. It should be noticed that the resonant tanks of the three phases have a common node. The three-phase midpoint marked as M in Fig. 1 can be directly connected to the ground or floated. The two derived structures are MPNFS and MPFS. Both of these structures allow for the benefits of the three-phase interleaved solution as shown in [25].

The main distinction of the two structures is that the MPFS should follow the current constrain of:

$$i_{rA} + i_{rB} + i_{rC} = 0 \tag{1}$$

An equivalent circuit of a single-phase LLC module is shown in Fig. 2 to evaluate the current balance performance. U_{res} is the voltage across the resonant inductor and resonant capacitor. U_{in} is the modulated output voltage of the switch array. U_T is the primary side voltage of the transformer. i_r, i_m and i_o are the resonant current, magnetizing current and output current. U_{mid} is the voltage of the midpoint.

For the convenience of analysis, the FHA method is used. In Fig. 2, according to KVL, the following phasor relationship should be satisfied:

$$\begin{cases} \vec{U}_{in} = \vec{U}_{res} + \vec{U}_T + \vec{U}_{mid} \\ \vec{i}_m = \vec{U}_T / jX_m \\ \vec{U}_{res} = \vec{i}_r jX_r \\ \vec{i}_r = \vec{i}_m + \vec{i}_o \end{cases} \tag{2}$$

It should be noticed that $\boldsymbol{U_{mid}}$=0 in MPNFS since the midpoint is directly connected to the ground. Meanwhile, $\boldsymbol{U_{mid}}$ has the same amplitude but a different phase under the reference phase of $\boldsymbol{U_{in}}$ in each phase. jX_r is the resonant impedance of the resonant tank, and jX_m is the magnetizing impedance, which can be calculated by:

$$\begin{cases} X_r = \omega_s L_r - \dfrac{1}{\omega_s C_r} \\ X_m = \omega_s L_m \end{cases} \tag{3}$$

ω_s represents the switching frequency, and X_r changes along with ω_s. This indicates that the fixed resonant parameter tolerance may result in different changes on X_r and X_m under different switching frequencies in the three phases.

X_{rk}(k=A,B,C) and X_{mk}(k=A,B,C) are the different resonant tank reactances of the three phases. Consider the condition that the switching frequency is higher than the resonant frequency. Then $\boldsymbol{U_{Tk}}$(k=A,B,C) have the same amplitudes since the transformers are always clamped by the paralleled output voltage. Moreover, $\boldsymbol{U_{ink}}$(k=A,B,C) have the same amplitude and a 120° phase-shift with respect to each other since they have the same frequency and duty cycle but a 120° phase-shift of the driving signals. This can be expressed by:

$$\begin{aligned} &\left|\vec{U}_{TA}\right| = \left|\vec{U}_{TB}\right| = \left|\vec{U}_{TC}\right| \\ &\vec{U}_{inB} = \vec{U}_{inA}\angle(-2\pi/3) \ , \ \vec{U}_{inC} = \vec{U}_{inB}\angle(-2\pi/3) \end{aligned} \tag{4}$$

Then the current of each phase can be calculated as follows.

A. Current Distribution in MPNFS

In order to calculate $|\boldsymbol{i_{rk}}|$, the current relationship in (2) can be used.

$$\begin{aligned} &\vec{i}_{rk} = \vec{i}_{mk} + \vec{i}_{ok} \\ &\Rightarrow \vec{i}_{rk} = \frac{\vec{U}_{Tk}}{jX_{mk}} + \frac{\vec{U}_{Tk}}{R_{lk}} \end{aligned} \tag{5}$$

R_{lk}(k=A,B,C) are the equivalent load resistances of each phase. R_{lk} also has a certain discrepancy due to the same output voltage and a different phase current. Equation (5) also shows that $\boldsymbol{i_{mk}}$ and $\boldsymbol{i_{ok}}$ are perpendicular to each other. Combining this with (2), the resonant current can be obtained as:

$$\vec{i}_{rk} = \vec{U}_{ink} / \left(jX_{rk} + \frac{jX_{mk}R_{lk}}{jX_{mk} + R_{lk}} \right) \tag{6}$$

To eliminate the influence of R_{lk} in (6), another equation can be obtained from Fig. 2 as follows:

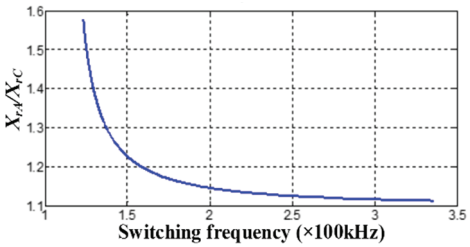

Fig. 3. Ratio of the resonant impedance.

$$\begin{aligned} &\left|\vec{U}_{Tk}\right| = \left|\frac{R_{lk} // jX_{mk}}{R_{lk} // jX_{mk} + jX_{rk}}\right| \left|\vec{U}_{ink}\right| \\ &\Rightarrow \frac{\left|\vec{U}_{ink}\right|}{\left|\vec{U}_{Tk}\right|} = \left|1 + jX_{rk}\left(\frac{1}{R_{lk}} + \frac{1}{jX_{mk}}\right)\right| = \sqrt{\left(1 + \frac{X_{rk}}{X_{mk}}\right)^2 + \left(\frac{X_{rk}}{R_{lk}}\right)^2} \end{aligned} \tag{7}$$

Combining (5), (6) and (7) yields:

$$\begin{aligned} &\left|\vec{i}_{rk}\right| = \frac{\left|\vec{U}_{Tk}\right|}{X_{rk}} \sqrt{\left(\frac{1}{m^2} - 1\right) - 2\frac{X_{rk}}{X_{mk}}} \\ &\left(m_k = \left|\vec{U}_{Tk}\right| / \left|\vec{U}_{ink}\right| \quad (\mathrm{k} = \mathrm{A,B,C})\right) \end{aligned} \tag{8}$$

The current ratio between different phases can be used to express the balance degree. Take phase A and phase C as examples. The resonant current ratio can be obtained as:

$$\frac{\left|\vec{i}_{rA}\right|}{\left|\vec{i}_{rC}\right|} = \frac{\dfrac{1}{X_{rA}}\sqrt{\left(\dfrac{1}{m_A^2} - 1\right) - 2\dfrac{X_{rA}}{X_{mA}}}}{\dfrac{1}{X_{rC}}\sqrt{\left(\dfrac{1}{m_C^2} - 1\right) - 2\dfrac{X_{rC}}{X_{mC}}}} \tag{9}$$

Equation (9) shows that the ratio of the resonant currents is influenced by three factors: 1) the resonant tank reactance, 2) the voltage gain, and 3) the ratio of the resonant tank reactance to the magnetizing reactance.

Since the transformer voltages are clamped to the output voltage in the most cases, the relationship $m_A \approx m_B \approx m_C$ can be obtained. The variation trends of X_{rk} and X_{mk} with different frequencies are obtained from (3). Take phase A and phase C as examples. The ratio of X_{mA} to X_{mC} is maintained while the ratio of X_{rA} to X_{rC} is changed when the switching frequency changes. The value of X_{rA}/X_{rC} under different switching frequencies is depicted in Fig. 3. The parameters are set to L_{rA}= 1.1L_{rB} = 11μH, C_{rA}=C_{rB}=200μF.

Fig. 3 shows that X_{rA}/X_{rB} experiences a dramatic increase around the resonant frequency. Therefore, when the switching frequency is close to the resonant frequency, the value of X_{rA}/X_{rB} becomes the main factor to determine the ratio of $|\boldsymbol{i_{rA}}|$ to $|\boldsymbol{i_{rC}}|$ according to the expression in (9). This means that the current distribution performance becomes worse around the resonant frequency under the same parameter difference.

Simulation results that depicts ratio of $|\boldsymbol{i_{rA}}|$ to $|\boldsymbol{i_{rC}}|$ under different loads in a three-phase LLC converter are shown in Fig. 4. The simulation is made under the conditions L_{rA}:L_{rB}:L_{rC}=(0.9:1:1.1), L_{rB} = 10μH, C_{rA}=C_{rB}=C_{rC}=200μF and L_{mA}=L_{mB}=L_{mC}=200μH.

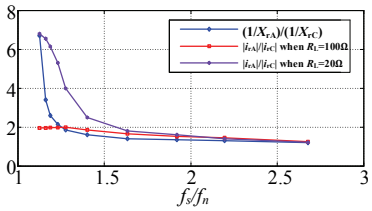

Fig. 4. $|\boldsymbol{i}_{rA}|/|\boldsymbol{i}_{rC}|$ with a variable switching frequency in MPNFS under different values of X_{rk}.

The simulation results in Fig. 4 show that the current balance performance in the three-phase MPNFS is dramatically worse when the load increases and the switching frequency approaches the resonant frequency.

B. Current Distribution of MPFS

Under the condition, $\boldsymbol{U}_{mid}$ can be calculated by (2):

$$\vec{U}_{mid} = -\frac{1}{3}\left[\left(\vec{U}_{TA}+\vec{U}_{TB}+\vec{U}_{TC}\right)+\left(\vec{U}_{resA}+\vec{U}_{resB}+\vec{U}_{resC}\right)\right] \tag{10}$$

In addition, the three phase current has the constraint shown in (1). This current can use a Fourier series expansion. In addition, since the different frequency components are orthogonal, the fundamental frequency also satisfies the following relation:

$$\vec{i}_{rA}+\vec{i}_{rB}+\vec{i}_{rC}=0 \tag{11}$$

Similar to MPNFS, the currents of the three phases can be calculated according to (10), (5) and (2). Take phase A as an example. This gives:

$$\vec{U}_{inA}/Z_A=\vec{i}_{rA}-\frac{1}{3}\left[\left(\frac{Z_B}{Z_A}-1\right)\vec{i}_{rB}+\left(\frac{Z_C}{Z_A}-1\right)\vec{i}_{rC}\right] \tag{12}$$

Z_k(k=A,B,C) in (12) can be expressed by:

$$\begin{cases} Z_k = jX_{rk}+\dfrac{jX_{mk}R_{lk}}{jX_{mk}+R_{lk}} \quad (k=A,B,C) \\ R_{lk}=1/\sqrt{\dfrac{\left|\vec{I}_{rk}\right|^2}{\left|\vec{U}_{Tk}\right|^2}-\left(\dfrac{1}{X_{mk}}\right)^2} \quad (k=A,B,C) \end{cases} \tag{13}$$

In addition, Z_k satisfies the following relationship:

$$\vec{I}_{rk}Z_k=\vec{I}_{rk}\left(jX_{rk}+\frac{jX_{mk}R_{lk}}{jX_{mk}+R_{lk}}\right)=\vec{U}_{resk}+\vec{U}_{Tk} \tag{14}$$

When compared with (6), equation (12) shows the coupling effect of the midpoint voltage in MPFS. After a proper simplification by combining (10), (13) and (14), equation (12) can be transformed to:

$$\left(\vec{U}_{inA}-\vec{U}_{mid}\right)/Z_A=\vec{i}_{rA}+\frac{1}{3}\left(\vec{i}_{rA}+\vec{i}_{rB}+\vec{i}_{rC}\right) \tag{15}$$

Generally, the parameter tolerance of each phase is small. Therefore, the magnitude of $\boldsymbol{U}_{mid}$ can almost be neglected when compared with $\boldsymbol{U}_{ink}$. Then (15) can be transformed to:

$$\vec{U}_{inA}/Z_A=\vec{i}_{rA}+\frac{1}{3}\left(\vec{i}_{rA}+\vec{i}_{rB}+\vec{i}_{rC}\right) \tag{16}$$

TABLE I
PARAMETERS FOR NUMERICAL CALCULATIONS

Specifications	Values
L_{rA},L_{rB},L_{rC}	8.1μH, 9μH, 9.9μH
C_{rA},C_{rB},C_{rC}	204nF, 204nF, 204nF
L_{mA},L_{mB},L_{mC}	150μH, 150μH, 150μH
U_{in}	400V

Equation (16) is more clearly compared to (12). This explains the current change principle when the system instantaneously changes from MPNFS to MPFS. Assuming the current has not changed at the beginning when the midpoint is floating, the relationship $\boldsymbol{i}_{rA}+\boldsymbol{i}_{rB}+\boldsymbol{i}_{rC}\neq\boldsymbol{0}$ exists. Then the three phase currents change based on the relationship in (16). Finally, when the currents satisfy the constraint of $\boldsymbol{i}_{rA}+\boldsymbol{i}_{rB}+\boldsymbol{i}_{rC}=\boldsymbol{0}$, the system reaches the steady state.

In order to compare the current distribution characteristic before and after the midpoint is floating, assume that the currents in MPFS are the same as the currents in MPNFS under the same parameter tolerance and switching frequency.

The current sum in (16) can be expressed by:

$$\vec{i}_{sum}=\vec{i}_{rA\_nf}+\vec{i}_{rB\_nf}+\vec{i}_{rC\_nf} \tag{17}$$

$\boldsymbol{i}_{rk\_nf}$ represent for the currents in MPNFS. Equations (6) and (7) are used to calculate the magnitude and phase angle of $\boldsymbol{i}_{sum}$.

The expressions of $\boldsymbol{i}_{rk\_nf}$ is:

$$\begin{cases} \left|\vec{i}_{rk\_nf}\right|=\dfrac{\left|\vec{U}_{Tk}\right|}{X_{rk}}\sqrt{\left(\dfrac{\left|\vec{U}_{ink}\right|^2}{\left|\vec{U}_{Tk}\right|^2}-1\right)-2\dfrac{X_{rk}}{X_{mk}}} \\ \angle\left(\vec{i}_{rk\_nf},\vec{U}_{ink}\right)=\angle\left[1-1/\left(1+jX_{rk}\left(\dfrac{1}{jX_m}+\sqrt{\dfrac{\left|\vec{i}_{rk\_nf}\right|^2}{\left|\vec{U}_{Tk}\right|^2}-\dfrac{1}{X_{mk}^2}}\right)\right)\right]-\dfrac{\pi}{2} \end{cases} \tag{18}$$

The numerical calculation used as the expressions in (18) are complex. The parameter relationship is set to be $\boldsymbol{X_{rA}<X_{rB}<X_{rC}}$, $\boldsymbol{X_{mA}=X_{mB}=X_{mC}}$. The employed parameters are presented in Table I.

The variables in (18) are the output voltage and switching frequency. Then according to (16) and (17), the value of $|\boldsymbol{i}_{rk\_nf}+(1/3)\boldsymbol{i}_{sum}|$, when compared with $|\boldsymbol{i}_{rk\_nf}|$, is taken into consideration. The results in phase A and phase C are presented in Fig. 5 since they have the maximum and minimum currents in the three phases.

f_s is the switching frequency and $f_n=f_{rB}$ is the resonant frequency of phase B. It can be concluded from Fig. 5 that if the currents in MPFS are equal to the current in MPNFS, $|\boldsymbol{i}_{rA\_nf}+(1/3)\boldsymbol{i}_{sum}|$ becomes higher than $|\boldsymbol{i}_{rA\_nf}|$ and $|\boldsymbol{i}_{rC\_nf}+(1/3)\boldsymbol{i}_{sum}|$ becomes lower than $|\boldsymbol{i}_{rC\_nf}|$ over a wide switching frequency and output voltage range. A phasor diagram is plotted in Fig. 6 to illustrate the results.

According to the numerical calculation results, when comparing the expressions in (16) and (6), it can be concluded that the current of phase A deceases and the current of phase

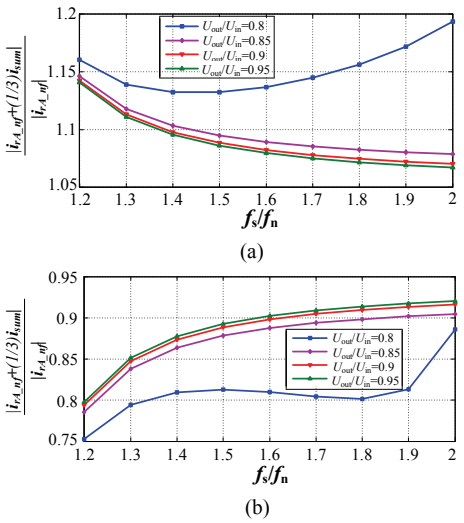

Fig. 5. Magnitude change of the current in phase A and phase C. (a) The value of $|\boldsymbol{i}_{\mathbf{rA\_nf}}+(1/3)\boldsymbol{i}_{\mathbf{sum}}|/|\boldsymbol{i}_{\mathbf{rA\_nf}}|$. (b) The value of $|\boldsymbol{i}_{\mathbf{rC\_nf}}+(1/3)\boldsymbol{i}_{\mathbf{sum}}|/|\boldsymbol{i}_{\mathbf{rC\_nf}}|$.

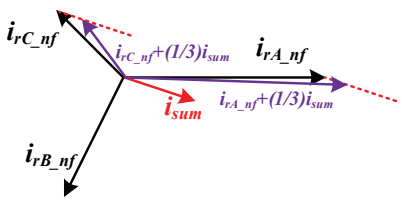

Fig. 6. Phasor diagram of $\boldsymbol{i}_{\boldsymbol{rk\_nf}}$ and $\boldsymbol{i}_{\boldsymbol{sum}}$.

C increases when the system changes from MPNFS to MPFS. This explains that the three phase currents have a higher balanced degree when $|\boldsymbol{i}_{\boldsymbol{rA}}|>|\boldsymbol{i}_{\boldsymbol{rB}}|>|\boldsymbol{i}_{\boldsymbol{rC}}|$ in general cases.

The influence of tolerance on L_{mk} can also be derived by a numerical method based on (18). Its influence gradually increases from a heavy load to a light load according to (5). Simulation results take the current ratio of phase A to phase C as example. The influence of the tolerance on L_{mk} is involved. This tolerance is expressed by L_{mA}:L_{mB}:L_{mC} = (1-p):1:(1+p), where p ranges from -20% to 20%. L_{rk} and C_{rk} are still equal to the values in Table I. Although the tolerance of the resonant inductance is fixed, X_{rk} changes along with the switching frequency. The results under the different cases are presented in Fig. 7.

From Fig. 7, it is observed that the maximum current error is about 20% under the different working states. The different value of X_{rk} is no longer the main factor to determine the current distribution. The current distribution does not have as big a change as in MPNFS when the switching frequency approaches the resonant frequency. In addition, under a heavy load, the influence of X_{mk} can also be neglected and the current has a high balance degree as shown in Fig. 7(a). However, under a light load, R_{lk} can be neglected and the current distribution is mainly determined by the difference in X_{mk} as shown in Fig. 7(c). These results verify that the three phase currents in MPFS have an inherent current sharing

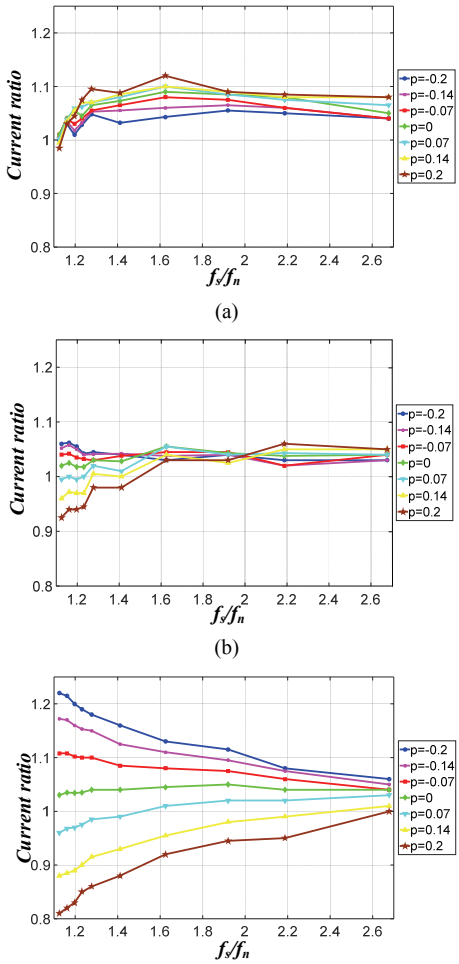

Fig. 7. $|\boldsymbol{i}_{\mathrm{rA}}|/|\boldsymbol{i}_{\mathrm{rC}}|$ under different switching frequencies and magnetizing inductance mismatch in MPFS. (a) R_l=10Ω. (b) R_l=30Ω. (c) R_l=100Ω.

capacity under unbalanced resonant parameters.

III. Optimal Phase Shift Control Method of the Midpoint Voltage Controllable Part

It has been demonstrated that the three phase currents still do not achieve complete balance by only floating the midpoint. Hence, a control method is added to achieve this purpose. This method is intended to add an extra phase shift among the three phase driving signals, which initially have a 120° phase angle with respect to each other. The goal is to add an extra midpoint voltage, which is expressed as $\Delta\boldsymbol{U}_{\mathbf{mid}}$.

The phase shifts of the driving signals indicate the phase shift among $\boldsymbol{U}_{\mathbf{ink}}$. Set the angle of $\boldsymbol{U}_{\mathbf{inA}}$ as the reference. Then the angles φ_1 and φ_2 are added to $\boldsymbol{U}_{\mathbf{inB}}$ and $\boldsymbol{U}_{\boldsymbol{inC}}$ respectively. For the convenience of analysis, the phasor expression form is changed into the trigonometric expression form. Then the additional midpoint voltage

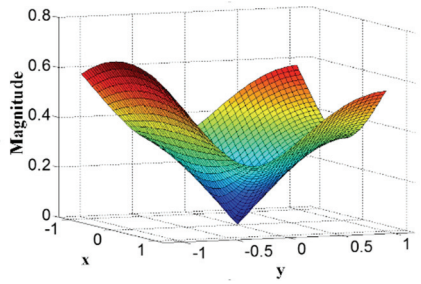

(a)

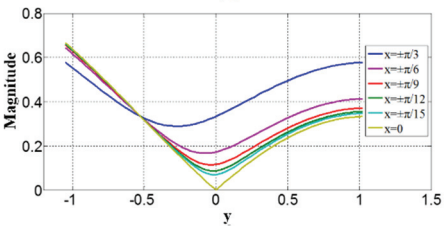

(b)

Fig. 8. Magnitude graph. (a) Variable x and y. (b) Different fixed x and variable y.

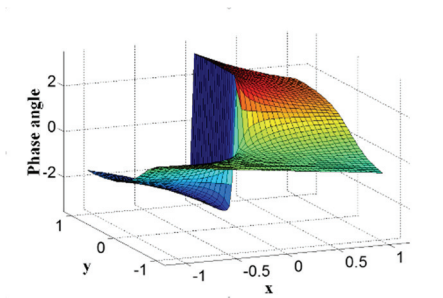

(a)

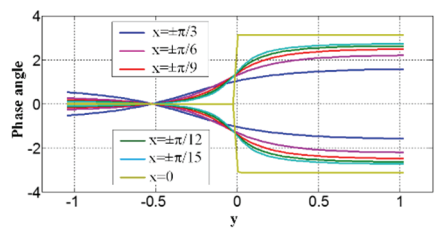

(b)

Fig. 9. Phase graph. (a) Variable x and y. (b) Different fixed x and variable y.

$\Delta \boldsymbol{U}_{\mathbf{mid}}$ can be calculated by:

$$\begin{aligned} 3\Delta\tilde{U}_{mid} &= U_{in}\sin[\omega_s t] + U_{in}\sin[\omega_s t - (\frac{2\pi}{3} + \varphi_1)] + U_{in}\sin[\omega_s t - (\frac{4\pi}{3} + \varphi_2)] \\ &= U_o[\sin\omega_s t \cdot (1 - 2\cos\frac{\varphi_1 + \varphi_2}{2}\cos(\frac{\varphi_1 - \varphi_2}{2} - \frac{\pi}{3}))] \\ &+ U_o[\cos\omega_s t \cdot (2\sin\frac{\varphi_1 + \varphi_2}{2}\cos(\frac{\varphi_1 - \varphi_2}{2} - \frac{\pi}{3}))] \end{aligned} \tag{19}$$

The employed parameter conversion is as follows:

$$\begin{aligned} & x = \frac{\varphi_1 + \varphi_2}{2}, y = \frac{\varphi_1 - \varphi_2}{2} \\ & \begin{cases} A = 1 - 2\cos x\cos(y - \frac{\pi}{3}) \\ B = 2\sin x\cos(y - \frac{\pi}{3}) \end{cases} \end{aligned} \tag{20}$$

Then the magnitude and phase angle of $\boldsymbol{\Delta U}_{\boldsymbol{mid}}$ are:

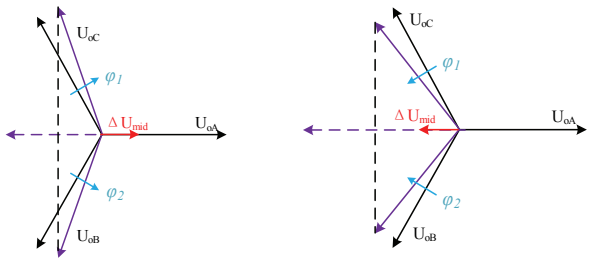

Fig. 10. Influence of the proposed phase change principle.

$$\begin{cases} \left|\Delta\vec{U}_{mid}\right| = \frac{1}{3}U_o\sqrt{A^2 + B^2} \\ \angle\Delta\vec{U}_{mid} = \arccos(\frac{A}{\sqrt{A^2 + B^2}}) \end{cases} \tag{21}$$

The magnitude and phase graph of $\boldsymbol{\Delta U}_{\boldsymbol{mid}}$ are depicted in Fig. 8 and Fig. 9, respectively. Fig. 8(a) and Fig. 9(a) are the three-dimension graphs. It is observed that the two graphs are symmetrical and antisymmetrical about the plane $x=0$. Graphs with a fixed x and a variable y are appended in Fig. 8(b) and Fig. 9(b).

It should be noticed that the phase graph is based on the reference phase of $\boldsymbol{U}_{\mathbf{inA}}$. When the reference is $\boldsymbol{U}_{\mathbf{inB}}$ or $\boldsymbol{U}_{\mathbf{inC}}$, the angle should be plus or minus 120°.

A. Proposed Control Method

Since three phase currents are coupled according to (1), only two addition control loops are necessary for current sharing. $|\boldsymbol{i}_{\mathbf{rA}}|$ and $|\boldsymbol{i}_{\mathbf{rB}}|$ are selected to be controlled variables.

Take the regulation of $|\boldsymbol{i}_{\mathbf{rA}}|$ as an example. In order to simplify the regulation to only one PI control loop that is easy to implement, one of the variables x and y should be fixed. It can be seen from Fig. 8(b) and Fig. 9(b) that one optimized choice is to set $x=0$. Under the condition where $\boldsymbol{\Delta U}_{\mathbf{mid}}$ and $\boldsymbol{U}_{\mathbf{inA}}$ are on the same straight line, $\boldsymbol{\Delta i}_{rA}$ and $\boldsymbol{i}_{rA}$ are almost on the same straight line as well. This means $\boldsymbol{\Delta U}_{\mathbf{mid}}$ can have the same influence on $|\boldsymbol{i}_{\mathbf{rA}}|$ with the minimum additional phase shifts. Meanwhile from Fig. 8(b), $|\boldsymbol{\Delta U}_{\mathbf{mid}}|$ can decrease to 0 only when $x=0$. Similarly, when the reference phasor is $\boldsymbol{U}_{\mathbf{inB}}$, the regulation of $|\boldsymbol{i}_{\mathbf{rB}}|$ has the same characteristic.

Therefore, the two balance control loops are established as follows based on setting $x=0$ and using a PI controller to regulate y.

1) The reference is $|\boldsymbol{i}_{rA}|$, the feedback is the mean value of $|\boldsymbol{i}_{\mathbf{rk}}|$(k=A,B,C). The control result is φ_{c1}, which means the additional phase shifts of phase B and phase C are $+\varphi_{c1}$ and $-\varphi_{c1}$, respectively.

2) The reference is $|\boldsymbol{i}_{\mathbf{rB}}|$, the feedback is the mean value of $|\boldsymbol{i}_{\mathbf{rk}}|$(k=A,B,C). The control result is φ_{c2}, which means the additional phase shifts of phase C and phase A are $+\varphi_{c2}$ and $-\varphi_{c2}$, respectively.

The effect of x=0 and the variable y can be more comprehensive by plotting the phasor diagram in Fig. 10. An overall control block diagram of the proposed current balance

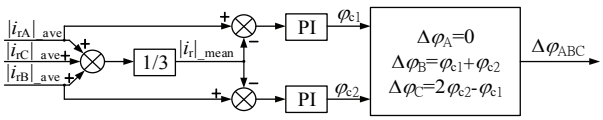

Fig. 11. Control block diagram of the proposed current balance method.

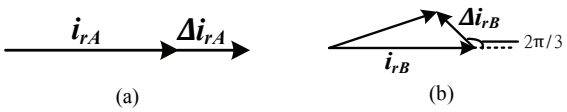

(a) (b)

Fig. 12. Current change with φ_{c1}. (a) Phase A. (b) Phase B.

principle is shown in Fig. 11. $|i_{rk}|_{ave}$ represents the mean value of $|i_{rk}|$. $\Delta\varphi_k$(k=A,B,C) are the final extra phase shift angles of each phase.

B. Coupled Factor

It has been demonstrated that the regulations of $|\boldsymbol{i}_{rA}|$ and $|\boldsymbol{i}_{rB}|$ have an influence on the other two other phases. Take phase A as an example. The required additional phase shifts are small since MPFS has a high degree of inherent current balance. Therefore, the assumptions $\sin\varphi_{c1}\approx\varphi_{c1}$ and $|\boldsymbol{i}_{rA}|\approx|\boldsymbol{i}_{rB}|$ are tenable. Then $|\Delta\boldsymbol{i}_{rA}|$ and $|\Delta\boldsymbol{i}_{rB}|$ are:

$$\left|\Delta\vec{i}_{rA}\right|=\frac{\left|\Delta\vec{U}_{mid\_A}\right|}{Z_{rA}+Z_{mA}//R_{LA}}=\left|\Delta\vec{U}_{mid\_A}\right|\left|\frac{\vec{i}_{rA}}{\vec{U}_{inA}}\right|=\frac{\sqrt{3}}{3}\varphi_{C1}\left|\vec{i}_{rA}\right|$$
$$\left|\Delta\vec{i}_{rB}\right|=\frac{\sqrt{3}}{3}\varphi_{C1}\left|\vec{i}_{rB}\right|\approx\left|\Delta\vec{i}_{rA}\right| \quad (22)$$

$|\boldsymbol{\Delta U}_{mid\_A}|$ is the additional midpoint voltage generated by the phase shift of φ_{c1}. Since $\boldsymbol{\Delta i}_{rA}$ and $\boldsymbol{i}_{rA}$ are on the same straight line, $\angle(\boldsymbol{\Delta i}_{rB}, \boldsymbol{i}_{rB})$=120° can be deduced. Phasor diagrams of the phase currents are depicted in Fig. 12.

It can be seen in Fig. 12 that $|\boldsymbol{i}_{rA}+\boldsymbol{\Delta i}_{rA}|>|\boldsymbol{i}_{rB}+\boldsymbol{\Delta i}_{rB}|$. Phase C has the same current change as phase B. This means $|\boldsymbol{\Delta U}_{mid\_A}|$ has a greater influence on $|\boldsymbol{i}_{rA}|$ than $|\boldsymbol{i}_{rB}|$ and $|\boldsymbol{i}_{rC}|$. Similarly, this conclusion can be expanded to the influence of φ_{c2}. $|\boldsymbol{\Delta U}_{mid\_B}|$ has a greater influence on $|\boldsymbol{i}_{rB}|$ than $|\boldsymbol{i}_{rC}|$ and $|\boldsymbol{i}_{rA}|$. Therefore, the system can finally realize current sharing despite the coupled factor. Meanwhile, a simple control model is derived from (22), where the control result is linear to the phase current. Since MPFS has an inherent high degree of current balance, the current balance loops can be designed to be far slower than the output voltage regulation loop. Then the stability of the system is not destroyed.

IV. Experimental Verification

A three-phase prototype has been built to validate the analysis and proposed control method presented in previous sections. The half bridge structures are used in both the primary side and secondary side of each phase.

Three LLC modules are prototyped using the specifications listed in TABLE II. The inductance of the resonant inductor and transformer excitation inductor are precisely measured by changing the air gap. Their inductances are equal in three phases. To make the results more convincing, the tolerance of the resonant capacitance is made to artificially enlarge the unbalance effect that is easier to figure out. Under this condition, $|\boldsymbol{i}_{mk}|$ are equal in three phases and the mean value of the three-phase rectified current on the transformer secondary sides, which are represented for $|\boldsymbol{i}_{ok}|$, are measured to derive the balance degree of the three phases. The prototype is shown in Fig. 13.

TABLE II
Key Parameters of the System

Symbol	Specifications	Values
f_s	Switching Frequency	130 kHz~200 kHz
U_{dc}	Input Voltage	250~400 V
U_{out}	Output Voltage	200~400 V
P_o	Output Power	3 kW
L_m	Magnetizing Inductance	100 μH
L_r	Resonant Inductance	7 μH
C_{rA},C_{rB},C_{rC}	Resonant Capacitance	138 nF,160 nF,182 nF
C_o	Output Capacitance	1000 μF

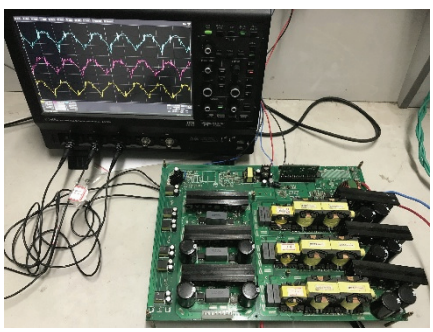

Fig. 13. Prototype of a three-phase LLC converter.

A. Inherent Current Balance Effect

The measured rectified three-phase secondary side current ($|\boldsymbol{i}_{oA}|$,$|\boldsymbol{i}_{oB}|$,$|\boldsymbol{i}_{oC}|$) of MPNFS and the primary side MPFS under the same working condition are depicted in Fig. 14.

The frequency is 140 kHz. The input and output voltage are 400 V and the load resistor is 50 Ω. When the system operates at around the three-phase resonant frequency, Fig. 14(a) shows a dramatically current unbalance in MPNFS. Phase A transmits nearly all of the active power of the converter to the output side. Before and after the midpoint is floating, the mean three-phase current changes from (17.2 A, 2.8 A, 2.4 A) to (4.6 A, 3.8 A, 4.0 A). The MPFS has an obviously high current balance degree.

The current ratio of phase A to phase C at different switching frequencies are depicted in Fig. 15.

Fig. 15 shows that in MPNFS, the phase current ratio is nearly equal to the ratio of the resonant tank impedance at a high switching frequency. Around the resonant frequency, the voltage drop on the line resistance cannot be neglect since the voltage across the resonant tank is very small. Under this

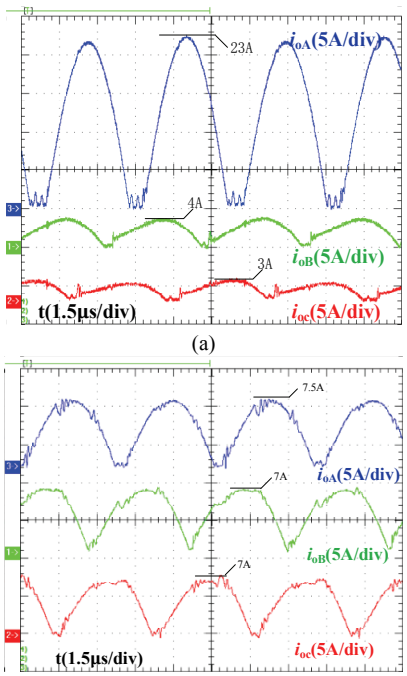

Fig. 14. Measured rectified three phase output current. (a) MPNFS. (b) MPFS.

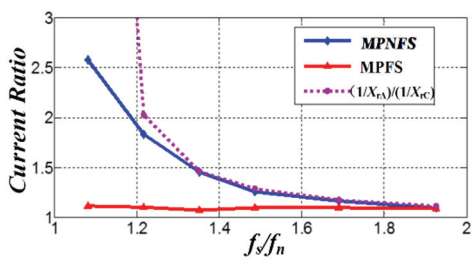

Fig. 15. Current ratio of phase A to phase C.

condition, the current ratio in a real system is restricted. However, it can be seen that the current ratio is always close to 1 in MPFS. Therefore, the inherent current balance characteristic of MPFS is clearly verified from Fig. 14(b) and Fig. 15.

B. Proposed Current Balance Control

Fig. 16 shows the balance process of the proposed current balancing method. The feedback currents i_{ok_ave} are the mean value of the measured rectified currents i_{ok} in Fig. 14.

In Fig. 16, before t_1, the system is stable. However, the balance control is not added, and the three phase currents are kept unbalanced. At t_1, the proposed control method is added and it can be seen that three-phase currents slowly approach their mean value. At t_2, the system has nearly realized current sharing. The balance control loop is much slower than the output voltage/current control loop since the balance duration of t_1~t_2 is nearly 850ms as shown in Fig. 16. Therefore, the output voltage is smooth during the whole progress and the stability of the converter is not affected. In addition, Fig. 17

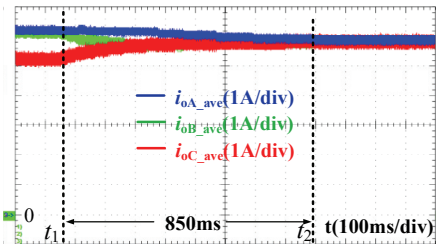

Fig. 16. Progress of the proposed control method.

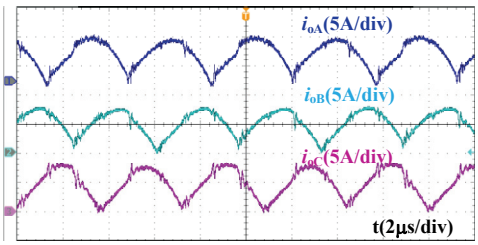

Fig. 17. Balanced current waveforms under full load.

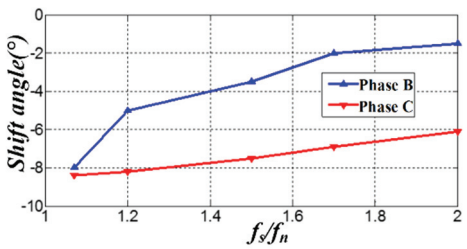

Fig. 18. Required additional shift angle of phase B and phase C.

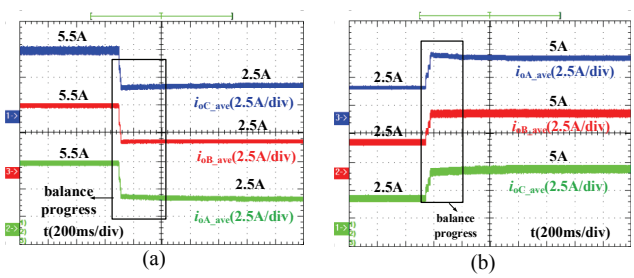

Fig. 19. Dynamic responses under load changes. (a) Full load to half load. (b) Half load to full load.

shows current waveforms of i_{ok} when the current sharing is realized under full load. The three-phase currents have the same mean value of about 5.5 A.

Set phase A as the reference. Then the additional phase shift angle of phase B and phase C at different switching frequencies are derived in Fig. 18. The required shift angles are really small as shown in Fig. 18. Therefore, the method is adapted to a wide range of parameter tolerances.

The small required additional phase shift angle means that the dynamic response is not significantly influenced. The dynamic responses under a fixed operating frequency are given in Fig. 19 and Fig. 20. Fig. 19 shows the current dynamic responses from full load to half load and from half load to full load, respectively. It can be seen that the phase currents are

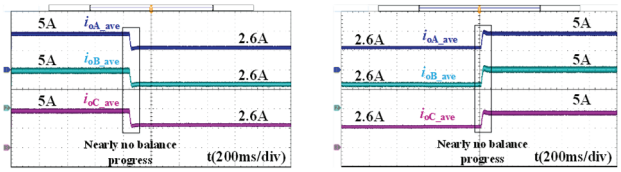

(a) (b)

Fig. 20. Dynamic responses under input voltage changes. (a) 400V to 250V. (b) 250V to 400V.

rapidly rebalanced after the load changes. Fig. 20 shows the current dynamic responses under input voltage changes between 400V and 250V. It can be seen that the balance state is nearly not influenced by the input voltage change.

V. Conclusions

This paper gives a solution for the current balance problem caused by the resonant parameter tolerance in three phase LLC converters. First, the structure is optimized by floating the midpoint of three phases. Under this condition, the current distribution characteristic of the converter is elaborated upon and a related method of phase shift control between modules is proposed. Some conclusions are summarized as follows.

1) In midpoint non-floating systems, the unbalanced degree dramatically increases, even under a small resonant parameter tolerance, when approaching the resonant frequency. The current distribution is mainly determined by resonant tank impedance which changes rapidly around the resonant frequency.

2) In midpoint floating systems, the current balance performance is better since the constraint that the sum of the three-phase current is zero. In addition, the midpoint voltage is inclined to balance the three-phase current.

3) The proposed control strategy adds two balance control loops. The magnitude and phase angle of the midpoint voltage are regulated to realize current sharing. Due to the inherent current balance characteristic in midpoint floating systems, the required additional phase shift angle is small. Thus, the stability and interleaved effect can be preserved.

Experimental results validate that three-phase current sharing is realized without adding extra components.

Acknowledgment

This work is supported by the National Key R&D Program of China (2018YFB0106300) and the National Natural Science Foundation of China (51777084).

References

[1] B. Yang, F. C. Lee, A. J. Zhang, and G. Huang, "LLC resonant converter for front end DC/DC conversion," in *Proc. 17th Annu. IEEE Appl. Power Electron. Conf. Expo. (APEC)*, pp. 1108-1112, 2002.

[2] B. Lu, W. Liu, Y. Liang, F. C. Lee, and J. D. van Wyk, "Optimal design methodology for LLC resonant converter," in *Proc. IEEE . Appl. Power Electron. Conf.*, pp. 533-538, 2006.

[3] J. Y. Lee, Y. S. Jeong, and B. M. Han, "An isolated DC/DC converter using high-frequency unregulated llc resonant converter for fuel cell applications," *IEEE Trans. Ind. Electron.,* Vol. 58, No. 7, pp. 2926-2934, Jul. 2011.

[4] M. Kim, "Two-phase interleaved LLC resonant converter with phase shedding control," in *Proc. Int. Power Electron. Conf.*, pp. 164-–1645, 2010.

[5] B.-R. Lin, W.-R. Yang, J.-J. Chen, C.-L. Huang, and M.-H. Yu, "Interleaved LLC series converter with output voltage doubler," in *Proc. Int. Power Electron. Conf.*, pp. 92-98, 2010.

[6] J. Deng, S. Li, S. Hu, C. C. Mi, and R. Ma, "Design methodology of LLC resonant converters for electric vehicle battery chargers," *IEEE Trans. Veh. Technol.*, Vol. 63, No. 4, pp. 1581-1592, Apr. 2014.

[7] J.-E. Yeon, W.-S. Kang, K.-M. Cho, T.-Y. Ahn, and H.-J. Kim, "Multiphase interleaved LLC-SRC and its digital control scheme," in *Proc. Int. Symp. Power Electron. Elect. Drives Autom. Motion*, pp. 1189-1193, 2010.

[8] B. C. Kim, K. B. Park, C. E. Kim, and G. W. Moon, "Load sharing characteristic of two-phase interleaved LLC resonant converter with parallel and series input structure," in *Proc. IEEE ECCE*, pp. 750-753, 2009.

[9] W. Martinez, M. Noah, S. Endo, K. Nanamori, S. Kimura, Y. Itoh, M. Yamamoto, J. Imaoka, and K. Umetani, "Three-phase LLC resonant converter with intergrateics," in *Proc. IEEE ECCE*, pp. 1-8, 2016.

[10] H. Figge, T. Grote, F. Schafmeister, N. Frohleke, and J. B ¨ ocker, "Two- phase interleaving configuration of the LLC resonant converter - Analysis and experimental evaluation," in *Proc. Ann. Conf. IEEE. Ind. Electron. Soc.*, pp. 1392-1397, 2013.

[11] H. S. Kim, J. W. Baek, M. H. Ryu, J. H. Kim, and J. H. Jung, "The high-efficiency isolated ac–dc converter using the three-phase interleaved LLC resonant converter employing the Y-connected rectifier," *IEEE Trans. Power Electron.,* Vol. 29, No. 8, pp. 4017-4028, Aug. 2014.

[12] F. Jin, F. Liu, X. Ruan, and X. Meng, "Multi-phase multi-level LLC resonant converter with low voltage stress on the primary-side switches," in *Proc. IEEE Energy Convers. Congr. Expo.*, pp. 4704-4710, 2014.

[13] O. Kirshenboim and M. M. Peretz, "Combined multi-level and two-phase interleaved LLC converter with enhanced power processing characteristics and natural current sharing," *IEEE Trans. Power Electron.,* Vol. 33, no. 7, pp. 5613-5620, Jul. 2017.

[14] E. Orietti, P. Mattavelli, G. Spiazzi, C. Adragna, and G. Gattavari, "Two phase interleaved LLC resonant converter with current-controlled inductor," in *Proc. IEEE Brazilian Power Electron. Conf.*, pp. 289-304, 2009.

[15] Z. Hu, Y. Qiu, and Y.-F. Liu, "A control strategy and design method for interleaved LLC converters operating at variable switching frequency," *IEEE Trans. Power Electron.,* vol. 29, no. 8, pp. 4426-4437, Aug. 2014.

[16] Y. Nakakohara, H. Otake, T. M. Evans, T. Yoshida, M. Tsuruya, and K. Nakahara, "Three-phase LLC series

resonant DC/DC converter using SiC MOSFETs to realize high-voltage and high-frequency operation," *IEEE Trans. Ind. Electron.,* Vol. 63, No. 4, pp. 2103-2110, Apr. 2016.

[17] C. Liu, X. Xu, D. He, H. Liu, X. Tian, Y. Guo, G. Cai, C. Ma, and G. Mu, "Magnetic-coupling current-balancing cells based input-parallel output-parallel LLC resonant converter modules for high-frequency isolation of dc distribution systems," *IEEE Trans. Power Electron.,* Vol. 31, No. 10, pp. 6968-6979, Oct. 2016.

[18] B. C. Kim, K. B. Park, C. E. Kim, and G. W. Moon, "Load sharing characteristic of two-phase interleaved LLC resonant converter with parallel and series input structure," in *Proc. IEEE Energy Convers. Congr. Expo.*, pp. 750-753, 2009.

[19] F. Duan, M. Xu, X. Yang, and Y. Yao, "Asymmetrical interleaving strategy and AVP concept for interleaved LLC resonant DC/DC," in *Proc. IEEE Appl. Power Electron. Conf.*, pp. 2003-2010, 2014.

[20] H. Wang, Y. Chen, Y. F. Liu, J. Afsharian, and Z. Yang, "A passive current sharing method with common inductor multiphase LLC resonant converter," *IEEE Trans. Power Electron.,* Vol. 32, No. 9, pp. 6994-7010, Sep. 2017.

[21] H. Wang, Y. Chen, Y. Qiu, P. Fang, Y. Zhang, L. Wang, Y.Liu, J. Afsharian, and Z. Yang, "Common capacitor multiphase LLC converter with passive current sharing ability," *IEEE Trans. Power Electron.,* Vol. 33, No. 1, pp. 370-387, Jan. 2018.

[22] M. Sato, R. Takiguchi, J. Imaoka, and M. Shoyama, "A novel secondary PWM-controlled interleaved LLC resonant converter for load current sharing," in *Proc. IEEE Int. Power Electron. Conf.*, pp. 2276-2280, 2016.

[23] H. Wu, X. Zhan, and Y. Xing, "Interleaved LLC resonant converter with hybrid rectifier and variable-frequency plus phase-shift control for wide output voltage range applications," *IEEE Trans. Power Electron.,* Vol. 32, No. 6, pp. 4246-4257, Jun. 2017.

[24] K. Murata and F. Kurokawa, "An interleaved PFM LLC resonant converter with phase-shift compensation," *IEEE Trans. Power Electron.,* Vol. 31, No. 3, pp. 2264-2272, Mar. 2016.

[25] E. Orietti, P. Mattavelli, G. Spiazzi, C. Adragna, and G. Gattavari, "Current sharing in three-phase LLC interleaved resonant converter," in *Proc. Energy Convers. Congr. Expo.*, pp. 1145-1152, 2009.

Lin Shi received his B.S. degree in Electrical Engineering from the Huazhong University of Science and Technology, Wuhan, China, in 2012, where he is presently working towards his Ph.D. degree in the School of Electrical and Electronics Engineering. His current research interests include high frequency ac/dc and dc/dc converters.

Bangyin Liu received his B.S., M.S. and Ph.D. degrees in Electrical Engineering from the Huazhong University of Science and Technology (HUST), Wuhan, China, in 2001, 2004 and 2008, respectively. He was a Postdoctoral Research Fellow in the Department of Control Science and Engineering, HUST, from 2008 to 2010. He is presently working an Associate Professor in the School of Electrical and Electronics Engineering, HUST. His current research interests include renewable energy applications, power quality and power electronics applied to power systems.

Shanxu Duan received his B.S., M.S. and Ph.D. degrees in Electrical Engineering from the Huazhong University of Science and Technology (HUST), Wuhan, China, in 1991, 1994 and 1999, respectively. Since 1991, he has been a Faculty Member in the College of Electrical and Electronics Engineering, HUST, where he is presently working as a Professor. His current research interests include stabilization, nonlinear control with application to power electronic circuits and systems, fully digitalized control techniques for power electronics apparatus and systems, and optimal control theory and its corresponding application techniques for high-frequency pulse width- modulation power converters. Dr. Duan is a Senior Member of the Chinese Society of Electrical Engineering; and a Council Member of the Chinese Power Electronics Society. He was selected as one of the New Century Excellent Talents by the Ministry of Education of China in 2007. He was also the recipient of the honor of "Delta Scholar" in 2009.